# Absolute, soft x-ray calorimetry on the Z facility at Sandia National Laboratories

D. L. Fehl, D. J. Muron, R. J. Leeper, G. A. Chandler,
C. Deeney, and R. B. Spielman
Sandia National Laboratories
Albuquerque, N. M. 87185
(505) 845-7822



## ABSTRACT

Simple and reliable x-ray *fluence* measurements, in addition to time-resolved diagnostics, are needed to understand the physics of hot Z-pinch plasmas. A commercially available laser calorimeter has been modified for measuring soft x-ray fluence from the Z facility at Sandia National Laboratories. The x-ray absorber of this calorimeter is an aluminum disk, attached to a two-dimensional thermopile and surrounded by an isoperibol shroud. The time-integral and the maximum of the thermopile voltage signal are both proportional to the x-ray energy deposited. Data are collected for 90 seconds, and the instrument has, thus far, been used in the 1 - 25 mJ range. A wider dynamic measuring range for x-ray fluence (energy/area) can be achieved by varying the area of the defining aperture. The calorimeter is calibrated by an electrical substitution method. Calibrations are performed before and after each x-ray experiment on the Z facility. The calibration of the time-integral of the thermopile voltage *vs.* energy deposited (or the peak of thermopile voltage *vs.* energy deposited) is linear with zero offset at the 95% confidence level. The irreproducibility of the calibration is <2%, and the imprecision in the measurement of the incident x-ray energy (inferred from signal noise and the calibration) is estimated to be ~0.9 mJ (95% confidence level). The inaccuracy is estimated at ±10%, due to correctable systematic errors (*e.g.*baseline shifts). Comparisons have been made of the calorimeter to time-resolved x-ray diagnostics, *e.g.*, bolometers and XRD (x-ray diode) arrays, by integrating the flux measured by these instruments over time.

## I. INTRODUCTION

Z-pinch plasmas have recently become intense sources of soft x rays (photon energies < ~2 keV). With peak x-ray powers > 200 TW[1] and yields of ~1.7 MJ based on a Lambertian model, imploding tungsten (W) wire arrays on the Z-facility (Sandia National Laboratories) have been proposed as drivers for radiation transfer experiments, inertial confinement fusion, and effects tests[2].

The dynamics of Z-pinch plasmas are, of course, probed by many diagnostics. But simple and reliable x-ray *fluence* measurements are needed to understand the physics of Z-pinch sources and to provide a comparison or check for more sophisticated, time-resolved, x-ray *flux* measurements -- a role emphasized here. For example, some x-ray diagnostics are calibrated on x-ray sources that are much less intense than a Z-pinch plasma. Other gauges may have no overall x-ray calibration or may be only relatively calibrated as a function of

## DISCLAIMER

photon energy. If the measured x-ray flux from such diagnostics can be integrated over a sufficiently long timescale and spectral bandwidth, the results may compared to an absolute, x-ray fluence measurement.

We have modified a commercially-available laser calorimeter[3] for measuring soft x-ray fluence on the Z facility (Z). Incident x rays are deposited in an absorber on a 10 ns time-scale, but the resulting thermal energy is measured over ~100 s interval with thermoelectric technology. One advantage of this approach is that the calorimeter does not have to discriminate a prompt x-ray signal from the intense, broad-band, electrical noise (EMP) also produced by the Z-accelerator. On the other hand, since μV electrical signals are obtained, its electronic components must *survive* the prompt noise. X-ray depositions of 1-25 mJ have been measured.

This paper describes the x-ray calorimeter developed for Z and its operation (§ II), discusses calibrations (§ III), and compares calorimetric x-ray fluence measurements with the time-integrated flux measurements from other diagnostics (§IV). Table I gives characteristics of the instrument.

## II. EXPERIMENTAL CONFIGURATION

Fig. 1 shows the energy detector[3] which is the basis for the soft x-ray calorimeter. A collimated beam of x-rays is absorbed in a (2.54 cm diameter x 0.5-mm-thick) aluminum disk (left). Thermal energy diffuses from this disk across a "thermal sandwich" and into an aluminum base. Wrapped around the absorbing disk is a small ohmic heater, used for calibrations. Fig. 1 also shows an aluminum shroud, which with the base nearly surrounds the energy detector with constant boundary (isoperibol) conditions. Isoperibol calorimeters are described by West[4].

The general operation of the calorimeter is sketched in Fig. 2. X rays of interest for Z-pinches have energies < a few keV and are deposited in the aluminum absorber within ~1 μm of the surface. Absorbed photon energy is quickly converted into thermal energy $\delta Q$, which diffuses to ambient conditions (in the base of the calorimeter) by thermal conduction through the thermal sandwich[3]. This structure consists of two outer, *electrically insulating* plates, separated by a regular, two-dimensional array of posts made of alternating thermoelectric materials. The posts are arranged in a square array and electrically connected in series, forming a thermopile. As thermal energy diffuses across the array, a spatially-varying temperature difference (proportional to the local thermal current) is produced across the posts. Such temperature differences generate proportional thermal emfs across pairs of posts (junctions), and the output signal $V_{th}(t)$ of the thermopile is the sum of these local thermal emfs. Thus $V_{th}(t)$ is proportional to the total heat current across the thermopile array, and $\int V_{th}(t)\, dt$ is proportional to $\delta Q$ deposited by x rays.

Some modifications were required to field the x-ray calorimeter on Z. As shown in Fig. 3, the calorimeter base and shroud is clamped between stainless steel retaining rings, attached to a 17.2-cm diameter vacuum flange by four equally-spaced rods. The ring closest to the entrance hole of the shroud contains the defining aperture: typically a 1-$cm^2$ steel aperture is used. A 3.2-mm thick teflon washer thermally isolates the radiated aperture ring from the isoperibol shroud. Near the base, the shroud has also been cut away to accommodate a permanent magnet, which applies a constant B field of ~5 mT (500 Gauss) parallel to the surface of the x-ray absorbing disk. This field returns photoelectrons emitted from the surface and sweeps out low energy charged particles. External electrical connections are made to the thermopile and the heater via high vacuum, coaxial SMA feedthroughs; both the center pin and shield of these connectors are electrically isolated from the vacuum flange and machine ground.

The calorimeter is fielded on Z at the end of a vacuum line of sight (LOS) pipe, 2245 cm from the source. 2 MJ of x rays radiated isotropically into $4\pi$ sr thus yield fluences of ~20 $mJ/cm^2$ at the detector. Typically, between Z shots the calorimeter is isolated from the LOS and maintained at pressures of ~1 x $10^{-6}$ Torr by its own turbo pumping system. Z shots are taken at ~5 x $10^{-5}$ Torr. In this range, heat transfer from the calorimeter by convection is negligible. Located between the calorimeter and the isolation valve is a fast-closure valve, which protects the detector from source-generated debris moving at ≤2.2 cm/μs. The fast valve also has a stainless steel aperture, which limits the x-ray beam at the defining aperture to a ~2.5 cm diameter circle. The calorimeter is aligned to the source before a shot series with a telescope. But the alignment is checked in each shot by attaching an *annular* piece of radiochromic film[5] over the defining aperture and observing later the region of full exposure.

Fig. 4 (right) sketches the electrical circuit for the thermopile. The μV signal from the calorimeter is conducted through high-vacuum feedthroughs to a dc amplifier,[3] located in a screen box, and the amplified, analog signal is digitized by a Tektronix 640A waveform digitizer, triggered externally. To reduce EMP noise, the input stage of the amplifier is buffered by shunt capacitance and in-line inductance; the zero-level is adjusted digitally. In addition, type RG-223, coaxial cable is used outside the vacuum; its shield is not grounded to the LOS pipe at the vacuum feedthroughs; rather, an auxiliary coaxial braid connects the pipe ground to the outer shield of the screen box. These precautions reduce the prompt noise signal to a high frequency, ~200-mV (p-p), ~8-μs burst.

## III. CALIBRATIONS

At Z, the calorimeter is calibrated *in situ* for each experimental shot: a full calibration of 13 points before the shot, and 6 points after the shot.

An electrical substitution method is used to calibrate the soft x-ray calorimeter. That is, known amounts of energy $E_{In}$ are introduced into the calorimeter by Joule heating of the

small wire wrapped around the outer perimeter of the absorber disk (Fig.1). The electrical circuit for this procedure is sketched in Fig. 4 (left). The heater has an ambient resistance of ~43 Ω and a low temperature coefficient of resistivity. The leads connecting the heater to the external circuit are optimized to limit parasitic voltage drops and thermal losses. During calibrations a 1%-precision current viewing resistor (CVR, 3.00 Ω) is located in a small, shielded box close to the vacuum interface, and the entire heater circuit is driven from the screen box (noted above) by a square-wave pulser, coupled to a power amplifier. Voltage measurements $V_{CVR}$ and $V_{TOT}$ are made across the CVR and CVR-plus-heater resistances, respectively, with connections close to the CVR (see Fig. 5). The energy $E_{In} = \int P_{In}(t)dt$, where the power in the heating pulse $P_{In}$ is $(V_{TOT} - V_{CVR})V_{CVR}/R_{CVR}$. Given adequate calibration of the CVR and digitizers, we believe that the uncertainties in $E_{In}$ can be ≤5%.

Figure 6 shows a family of cooling curves $V_{th}(t;E_{In})$ for a sequence of electrical heating pulses. Each curve has the same form out to ~60 s, where noise begins to dominate the traces; that is, $V_{th} = A(E_{In})f(t)$, where $f$ is a function of time $t$. A least-squares analysis shows that $f$ is approximated by

$$V_{th}(t;E_{Inp}) = A(E_{Inp})\left[e^{-t/\tau_1} - e^{-t/\tau_2}\right] \qquad (1)$$

where $\tau_1$ is a fall-time, $\tau_2$ is a rise-time, and $\tau_1 \gg \tau_2$. For example, for $E_{In}$ = 25 mJ the inset graph in Fig. 6 shows the quality of the fit with $\tau_1$ = 12.54 ± 0.06 s and $\tau_2$ = 0.77 ± 0.02 s), where the uncertainties are estimated at the 95% (2σ) confidence level[6]. As a check, one can calculate from Eq. (1) the time $t_p$ at which $V_{th}$ attains its peak value $V_p$ : that is, $t_p = ln(\tau_1/\tau_2)/(1/\tau_2 - 1/\tau_1)$. With the parameters just obtained $t_p$ = 2.3 s, which compares well with the data.

Several other characteristics of calibrational cooling curves are pertinent. (1) Small baseline offsets (~0.1 - 0.4 mV) occur in $V_{th}(t)$ after the heater is pulsed. These are estimated from the average signal level between 80-90 s in the cooling curve when the thermopile output is down to ~0.5% of $V_p$ and the recorded trace is noise. Offsets may be either positive or negative relative to the initial baseline, appear to be uncorrelated with the value of $E_{In}$, and are subtracted out before any analysis. (2) The fit parameters $\tau_1$ and $\tau_2$ may vary by several per cent within a calibration; such fluctuations also appear to be independent of $E_{In}$. (3) $\tau_1$ and $\tau_2$ differ between calibrations and x-ray exposures. (See below.)

Our calibrational procedure correlates $\int V_{th}\,dt$, obtained from cooling curves (Fig. 6), with $E_{In}$, inferred from heater pulses (Fig. 5). In the 0 - 25 mJ range this yields a linear function $A(E_{In})$ in Eq. (1). Thus, $\int V_{th}\,dt = A(E_{In})\cdot\int f\,dt = b_0 + b_1 E_{In}$. Fig. 7 shows 3 calibrations obtained over a 3 month period. An unweighted, linear least squares analysis of all the data points gives $b_0$ = 0.0021 ± 0.0122(2σ)V-s and $b_1$ = 0.04243 ± 0.00082(2σ)V-s/mJ. The uncertainties are estimated from the fit residual. The uncertainty in $b_0$ is consistent with the hypothesis that $b_0 \equiv 0$ (95% confidence), and the uncertainty in $b_1$ gives an estimate of ~ 2% for the irreproducibility of the calibrations[6]. The dashed curves in Fig. 7

represent the overall ($2\sigma$) uncertainty in the fit.[6]

If $\int V_{th}\, dt$ is directly proportional to the energy deposited in the calorimeter *by whatever means*, the calibration curve in Fig. 7 can be inverted to obtain the x-ray energy absorbed in the calorimeter for experiments on Z. Thus, $\delta Q$(mJ) = -0.0546 + 23.577 $\int V_{th}\, dt$ (V-s) for this calibration. If one assumes that uncertainties in $\int V_{th}\, dt$ are similar for both calibrational and x-ray data, then a 2-$\sigma$ estimate[6] of the imprecision in $\delta Q$ is ~0.9 mJ, which varies by < 4% over the range 0 - 25 mJ.

Although electrical calibration data are taken with each Z shot, Fig. 7 shows that the fitted calibration is relatively stable with time. Thus, it is often unnecessary to construct a new inverse regression for each shot. Rather, it is simpler and more precise to check each new calibration against an average (standard) calibration and to calculate $\delta Q$ from the standard calibration until a statistically significant change occurs. In fact, such *checks of a calibration* need not even be done with $\int V_{th}\, dt$; one can regress $V_p$ on $E_{In}$ since the peak signal is related to both $A(E_{In})$ and $\int V_{th}\, dt$ by Eq. (1):

$$V_p = A(E_{Inp})\, e^{-t_p/\tau_1}[1 - \tau_2/\tau_1] = e^{-t_p/\tau_1} \int_0^\infty V_{th}(t)dt\ /\tau_1\ . \qquad (2)$$

For the cooling curves in Fig. 6, one finds the ratio $\int V_{th}\, dt$ / [$V_p\ \tau_1 \exp(t_p/\tau_1)$] to be 1.01 ± 0.037 ($1\sigma$). On the other hand, *inverse predictions* $\delta Q$ based on $V_p$ require an ~10% correction because the cooling curve shapes differ between calibrations and x-ray shots and are thus generally not made.

## IV RESULTS AND DISCUSSION

The soft x-ray calorimeter has been fielded on over 50 shots at Z (LOS 5/6). Fig. 8 shows the cooling curve $V_{th}\ (t\ )$ for an early shot (Z-126, 18 September 1997). One sees a data peak at ~28 mV above the initial baseline with a signal-to-noise ratio of ~50. There is also a post-shot baseline shift of 0.45 mV. Subtracting this offset (as above), one obtains $\int V_{th}\, dt$ = 0.49 V-s. The calibration and the aperture area (1 cm$^2$) then yield a measured fluence of 11.5 ± 0.9 ($2\sigma$) mJ/cm$^2$ -- a typical, mid-range shot. To make sure that such signals are due to x rays and not EMP or heating of nearby objects, the defining aperture was replaced in shot Z-128 with a solid plate, of the same thickness as the normally fielded aperture. The signal for this background test is also shown in Fig. 8, and only noise is visible. Other diagnostics showed that shot Z-128 yielded about half the output of Z-126.

We have assumed that the processes of introducing thermal energy into the calorimeter by Joule heating and x-ray deposition are *equivalent*. Thus, calibrations like Fig. 7, performed electrically, were inverted to infer the energy deposited by x rays. Yet the cooling curves $V_{th}\ (t\ )$ from calibrations and x-ray exposures differ subtly in two ways: post-shot

offset and shape. How can these differences be understood, and do they affect the assumption of equivalence?

Late-time offsets are more prominent for x-ray deposition than for calibrations. For x ray experiments they range from ~0.5 - 2 mV and are positive relative to the initial baseline, while the corresponding baseline shifts for calibrational data may be one-tenth as large and (as noted above) either positive or negative. The importance of this feature is that although an offset may be a relatively small fraction of $V_p$ , it can perturb $\int V_{th}\, dt$ significantly. For example, in Fig. 8 $\int V_{th}\, dt$ and $\delta Q$ would be ~10% larger if the 0.45-mV offset were ignored. We have treated offsets as systematic errors and subtracted them from the cooling curves of both calibrations and x-ray exposures, so that equivalence is unaffected. Once this correction is made, one can usually obtain consistent fit parameters $\tau_1$ and $\tau_2$ and agreement of $\int V_{th}\, dt$ with Eq. (2).

The source of post-shot offsets is not yet clear. We find no correlation between the magnitude of the shift and $\delta Q$, nor between such offsets and fluctuations in the shape of $V_{th}$ ($t$). If anything, the offsets appear to depend on the area of the defining aperture: negligible in the background shot and ~2 mV for the largest aperture (3.1 cm$^2$), used when $\delta Q \leq 1$ mJ. Another clue is that we have captured a similar offset in pre-shot trigger checks on Z (Fig. 8, inset), when no electrical energy is delivered to the Z-pinch load but all the command triggers are fired and fast valves closed. During these tests and perhaps during real shots, EMP signals may somehow be getting past the input filtration of calorimeter amplifier and resetting the digital zero. If so, one might correct the cooling curves by subtracting the signal in Fig. 8, scaled to fit the late-time shift. Alternatively, the thermopile may act as a stress gauge, shifting its output whenever mechanical vibrations interact with it. This issue is still under investigation.

Base-corrected cooling curves from x-ray exposures can be fit by the double exponential function of Eq. (1). For x-ray exposures $\tau_1 = 13.99 \pm 0.28(1\sigma)$ s and $\tau_2 = 1.35 \pm 0.12\ (1\sigma)$ s, averaged over 15 shots. Both parameters are thus larger than the corresponding values from calibrations: $\tau_1$ by ~12% and $\tau_2$ by ~75%. The peak time $t_p$ also increases from 2.3 to 3.5 s. A qualitative explanation for these differences is that thermal energy is deposited in the calorimeter differently in the two cases. For x-ray exposures the dose is deposited within ~1 μm of the front surface of the aluminum absorber disk; energy then diffuses through the disk to the thermal sandwich. For electrical calibrations, heat enters both the absorber and the sandwich along the periphery of the disk. One thus intuitively expects smaller time constants for the calibrational case since the path to the thermopile is shorter. This heat flow problem is being studied quantitatively[7]. Equivalence between the two methods of deposition is not threatened if the shape of the cooling curve is the *only* difference: by either mechanism $\int V_{th}\, dt$ should be proportional to the energy and thus independent of curve shape.

Thermal energy loss mechanisms have also been studied as a possible source of non-equivalence between x-ray and electrical heating processes. Although the calorimeter is nearly surrounded by an isoperibol shroud, *some* energy does bypass the thermal sandwich and is not measured in $\int V_{th}\, dt$, *no matter how deposited.* In particular, unlike conduction through lead wires and convection, radiant thermal transport is not restricted in the as-fielded calorimeter. The question of equivalence then depends on whether such losses are significant and, if significant, whether they differ appreciably between the two deposition processes. We consider only the x-ray deposition process, for which one intuitively expects the larger radiant losses. In this case energy is absorbed close to the front surface of the calorimeter, yielding relatively high, initial, surface temperatures. (See below.) Fortunately, the conductive heat current in the aluminum absorber from the surface is many orders of magnitude larger than radiative current due to the Stefan-Boltzmann law, and the integrated radiant losses are small. A simple, thermal conduction model of the absorber shows that <1% of the fluence of x rays is lost to thermal radiation. Thacher[8] has shown experimentally for similar laser calorimeters that equivalence between Joule- and x-ray heating is valid within 2%.

Surface blowoff and hot gases are two other potential perturbations to the as-fielded calorimeter. If the surface dose of x rays to the absorber exceeds the enthalpy of aluminum to vaporization, some of the incident x-ray energy will be carried away by surface blowoff, giving a negative systematic error. We estimate ~40 mJ/cm$^2$ as a conservative limit for aluminum on Z. Larger fluences may be accommodated by imaging the source or coating the absorber with beryllium or diamond. Another perturbation occurs if hot gases from the source or blowoff from other surfaces reach the absorber, giving a positive bias. Visual inspections of the absorber reveal no surface contamination. We are also developing a fast surface-temperature gauge to detect hot gases[7].

X-ray fluence measurements made by the calorimeter have been compared with the time-integrated flux from two other diagnostics. The first is a filtered array of x-ray detectors (XRDs)[9,10]. These gauges are vacuum photodiodes, in which a collected electron current is directly proportional to the incident x-ray flux. Reconstructing the flux explicitly, however, requires a timewise unfold of the signals since the spectral response of each XRD channel is strongly energy dependent. X-ray fluence is obtained by integrating the time-dependent flux. XRDs are calibrated at a synchrotron x-ray source. The second diagnostic is an x-ray bolometer[11]. In this detector the accumulating x-ray deposition heats a 1-μm-thick Ni film, the temperature of which is measured as a change of resistance. The incident x-ray fluence is then derived from the resistance of the gauge before and after x-ray exposure. Its calibration depends on published values of thermophysical constants as a function of temperature and a theoretical model.

At Z two co-located bolometers, the calorimeter, and a 5-channel array of XRDs are routinely fielded on the same LOS. Distances $r$ to the source are 1895 cm, 2245 cm, and 2395 cm, respectively; differences in viewing angle are <1°. Sometimes a second XRD array is fielded at $r$ = 1910 cm to check for scattered x rays; such "pipe shine" can cause the x-ray fluence to vary differently from $1/r^2$.

Figure 9 compares x-ray fluence measurements from these gauges on several Z shots. The abscissa of each point is the fluence measured by the soft x-ray calorimeter, and the ordinate (on two separated scales) is the fluence measured by either the XRD array (bullets, right) or the bolometers (asterisks, elevated, left), but *scaled* by $1/r^2$. All the fluence measurements thus refer to the same distance from the source and require no model for the source. The two off-axis, solid lines in the figure represent equality between the measurements and are meant to guide the eye. The measurements range from ~1 -25 mJ/cm$^2$ due to different sources (pinches and hohlraums) and front-end apertures. The meaning of the error bars varies with the detector; all are estimated at the 95% confidence level (2σ). For the calorimeter the uncertainties represent the imprecision of the measurement (~0.9 mJ/cm$^2$), estimated from the data and the calibration. Similarly, the errors (~24%) in the XRD measurements are largely due to calibrations. Uncertainties in the bolometers (~20%) estimate the disagreement between the two bolometers.

Some interesting conclusions come from this comparison. First, the calorimeter and bolometers are in close agreement. Statistically, the ratio $F_{bolometer}/F_{calorimeter}$ is 0.944 ± 0.066 (2σ), which just barely includes 1. (The anomalous point at ($F_{bolometer}$ =17.54 and $F_{calorimeter}$ = 6.01 has not been included.) The bolometer measurements have not been corrected for losses due to the x-ray transmission (> 1 keV) through the Ni film or thermal diffusion into the substrate; together these losses are estimated at ~5% and would bring the calorimeter and bolometer measurements into closer agreement.

A second conclusion is that the calorimeter and XRD measurements show a larger systematic disagreement. Here the ratio $F_{XRD}/F_{calorimeter}$ = 0.834 ± 0.038 (2σ). Simulations with black body spectra suggest a (negative) bias of ~ 0-10% in the unfolded XRD *flux* due to photons outside the acceptance band of the XRD array and to unfold errors. This bias is a function of the spectral shape at any given time. With time-dependent simulations, one can understand *fluence* ratios $F_{XRD}/F_{calorimeter} \approx 0.85$ - 0.92 by these mechanisms. The scatter in the XRD points may thus be due more to spectral differences than to calibration uncertainties.

The last conclusion one can draw from Fig. 9 relates to the issue of pipe shine. In eight of the Z-pinch shots two arrays of XRDs (primary and secondary) were simultaneously fielded at different distances. The ratio $F_{XRD\text{-}primary}/F_{XRD\text{-}secondary}$ for these shots is 1.060 ± 0.072 (2σ), where both fluence measurements have been scaled to the calorimeter distance. There is thus no statistical reason to suppose that x-ray fluences scale differently than $1/r^2$ within a resolution of ~7% at the 95% confidence level.

Besides continued characterization, future plans for the soft x-ray calorimeter include fielding several more such diagnostics on Z, including one instrument located 627 cm from the source with a near axial field of view. Fielding on filtered Z-pinches at the SATURN facility is also planned.

## ACKNOWLEDGMENTS

It is a pleasure to acknowledge the help of P. Thacher (Sandia National Laboratories) and N. R. Keltner (K-Tech). This work was supported by the U. S. Dept. of Energy under Contract DE-AC04-94AL85000. Sandia is a multiprogram laboratory operated by Sandia Corporation, a Lockheed Martin Company, for the U. S. Dept. of Energy.

Table 1. Summary of calorimeter properties.

| Properties | | Comments | Section Discussed |
|---|---|---|---|
| Energy Range | 1 -25 mJ | present calibration. | §III |
| Fluence Limits | ~0.3 mJ/cm$^2$ | calibration and aperture diameter. | §III |
| | ~40 mJ/cm$^2$ | front surface blowoff. | §IV |
| Imprecision | ~0.9 mJ | 95% confidence limits on inverse prediction from calibration. | §III |
| Correctable Biases | ~10% (mid-range) | ~1.5 mV post-shot baseline shift. | §III,IV |
| Irreproducibility | ~2% | 95% confidence limits on the calibration constants. | §III |

References

1. R. B. Spielman, et. al., *Phys. of Plasmas* **5** (1998).
2. M. K. Matzen, *Phys. of Plasmas,* **4(5)** (1997) 1519.
3. Scientech, Inc., 5649 Arapahoe Av., Boulder, CO, 80303-1399. Some parts of this instrument are considered proprietary by the company; inquiries should be addressed to Scientech. Use of any commercial product by Sandia National Laboratories does not constitute an endorsement.
4. E. D. West and K. L. Churney, *J. Appl. Phys.* **4(6)** (1970) 2705.
5. W. L. McLaughlin, et. al., *Nucl. Instrum. Meth.* **A302** (1991) 165.
6. M. G. Natrella, *Experimental Statistics Handbook* (U. S. Dept. of Commerce, National Technical Information Service, Springfield, VA; 1991) PB93-196038.
7. N. R. Keltner, Ktech Corp. (901 Pennsylvania Ave. NE, Albuquerque NM 87110), private communication.
8. P. Thacher, Sandia National Laboratories, private communication.
9. G. A. Chandler, et. al. *Rev. Sci. Instrum.* **63** (1992) 4828.
10. D. L. Fehl, et. al., *Rev. Sci. Instrum.* **68** (1997) 843.
11. D. L. Hanson, "User's guide to the SNL bolometers," (Sandia National Laboratories, Albuquerque, NM 87185; 8 February 1984), unpublished.

Figure Captions

1. The commercially-available calorimeter. At the left is the energy detector. X rays interact with an aluminum absorber disk at the top, which is mounted to a (square) thermal sandwich. A small heater wire is visible wrapped around the disk. The thermal sandwich is mounted to an aluminum base, 3 cm high and ~ 6 cm in diameter. On the right is an aluminum shroud which fits on top of the energy detector; the shroud is 7 cm long, with an outer diameter of 6 cm and an inner diameter of 3 cm.

2. Schematic of the energy detector, viewed from the side, to illustrate heat flow in the instrument. X rays deposit energy $\delta Q$ near the front surface of the absorber, and thermal energy diffuses across the absorber, two electrical insulators, and a two-dimensional thermopile array (meandering structure) into an aluminum base at ambient temperature $T_0$ . The insulators and thermopile constitute the "thermal sandwich." The thermal current $q$ varies spatially in the plane of the thermopile $(x,y)$ and produces a spatially-varying temperature gradient $\Delta T$ across the junctions. The resulting emfs are added, and the output voltage is proportional to the total thermal current across the thermopile. Energy can also be introduced by Joule heating in the ohmic heater wire, wrapped around the absorber.

3. Cut-away view of the as-fielded soft x-ray calorimeter. X rays enter from the left.

4. Electrical circuits for the calorimeter. The circuit at the right shows the

connection of the thermopile to the recording system, located remotely in a screen box. Most of the leads are coaxial cables with no connections to machine ground. An additional coaxial braid connects the LOS pipe (machine ground) to the outside of the screen box. Vacuum-tight SMA feedthroughs pierce the vacuum interface. At the left is the heater circuit used for electrical calibrations. A 20-ms-wide, square-wave pulse from a Stanford DG-535 pulser is amplified by a Kepco ATE15-3M power amplifier to drive the heater circuit. The electrical potential is measured across a precision current viewing resistor (CVR) and the ohmic heater.

5. Heater pulses $-V_{tot}(t)$ and 10 x $V_{CVR}(t)$ for noted input energies in the ohmic heater. The pulse width (20 ms) is < 1/30 of the risetime of the calorimeter (0.75 s).

6. A sequence of response (cooling) curves from the calorimeter for noted amounts of input energy in the ohmic heater (electrical calibration). All the curves have approximately the same double exponential shape and can be fit with two time constants ($\tau_1$ and $\tau_2$) and a scale factor. The inset show the quality of the fit for an input energy of 25 mJ.

7. Comparison of three electrical calibrations spanning a 3 month period. The solid line is a linear fit to the combined data set, and the dashed lines are the 95% confidence limits to the entire fit line.

8. Response (cooling) curve for Z-shot 126. A post-shot offset is noted and subtracted in the data analysis. Also shown is the result of a background shot, in which the defining aperture was blocked to x rays. The inset shows the thermopile signal from a trigger check, in which no x rays were produced by the source.

9. Comparison of calorimeter fluence measurements with time-integrated flux measurements from XRD arrays and bolometers. The abscissa of each point refers to the calorimeter measurement; but since the measurements overlap, the ordinates of the XRD and bolometer measurements are separated: bolometers (asterisks) left scale, XRDs (bullets) right scale. The two diagonal lines represent equality on corresponding scales. Since the XRDs and bolometers are not co-located with the calorimeter, these flux measurements have been scaled to the calorimeter distance by $1/r^2$. For some of the shots, two XRD arrays were used at different distances to check for "pipe shine"; in this case two XRD points are plotted for the same calorimeter value.

Fig 1

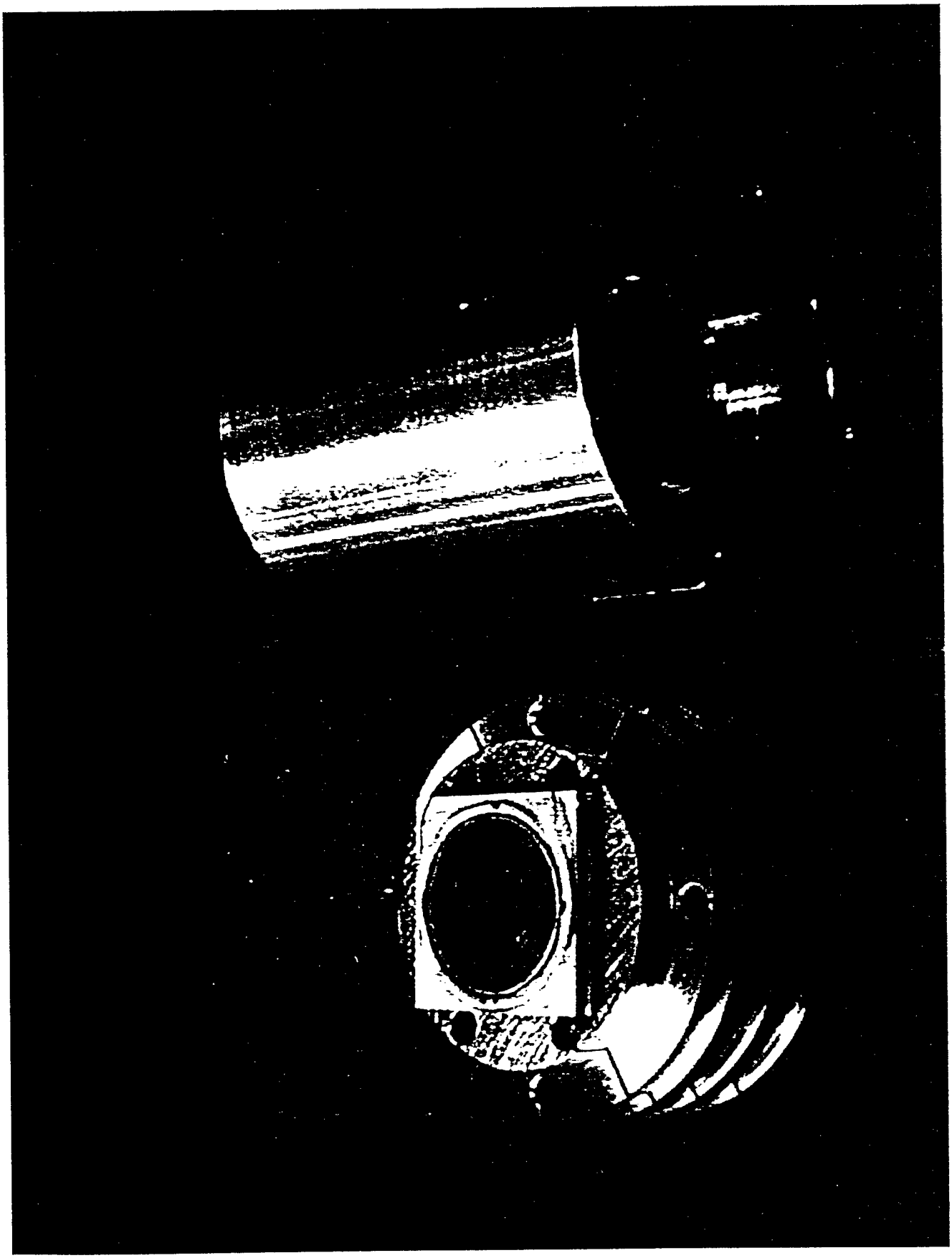

Fig 2

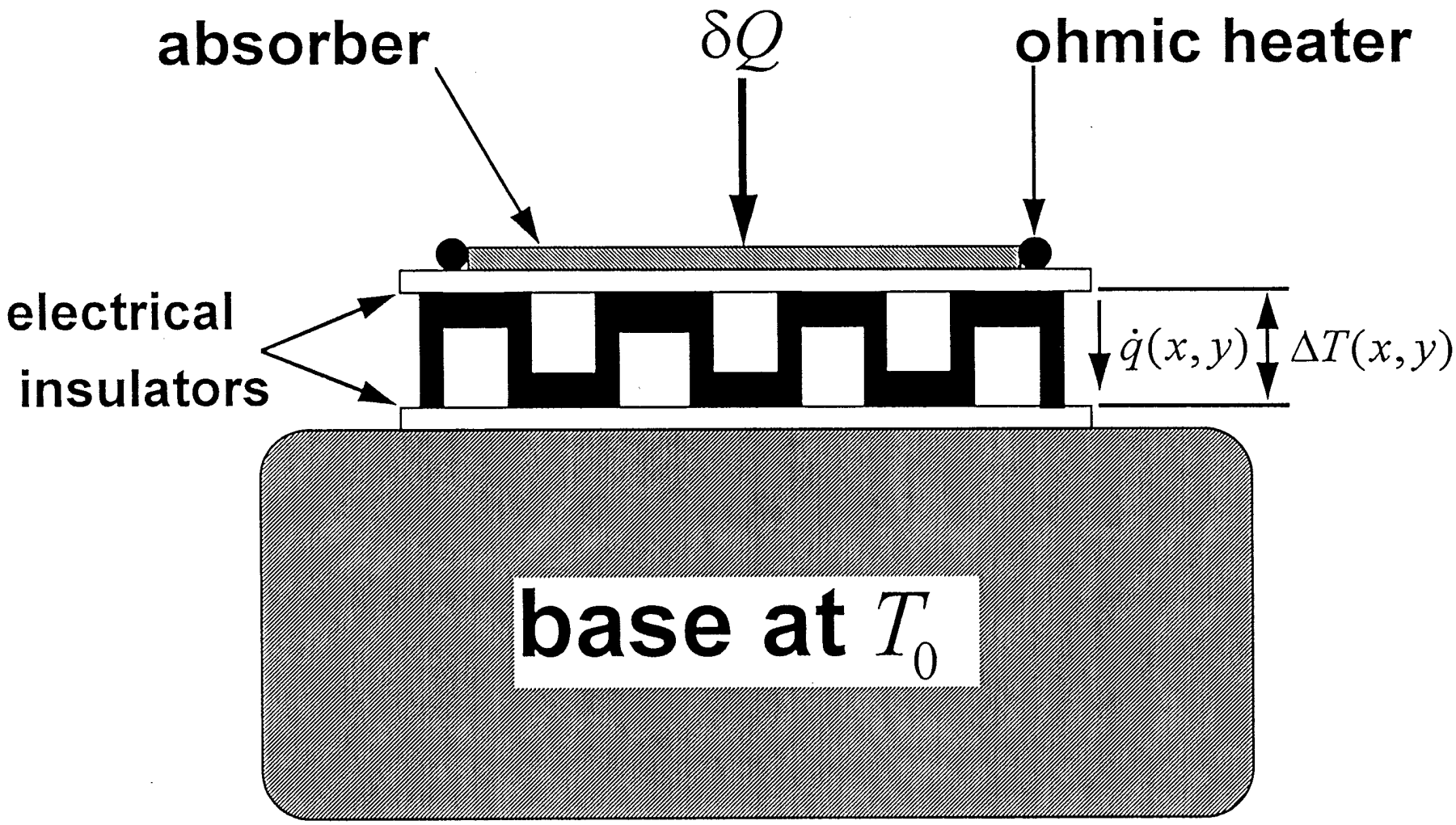
absorber
$\delta Q$
ohmic heater
electrical
insulators
$\dot{q}(x,y)$
$\Delta T(x,y)$
base at $T_0$

Fig 3

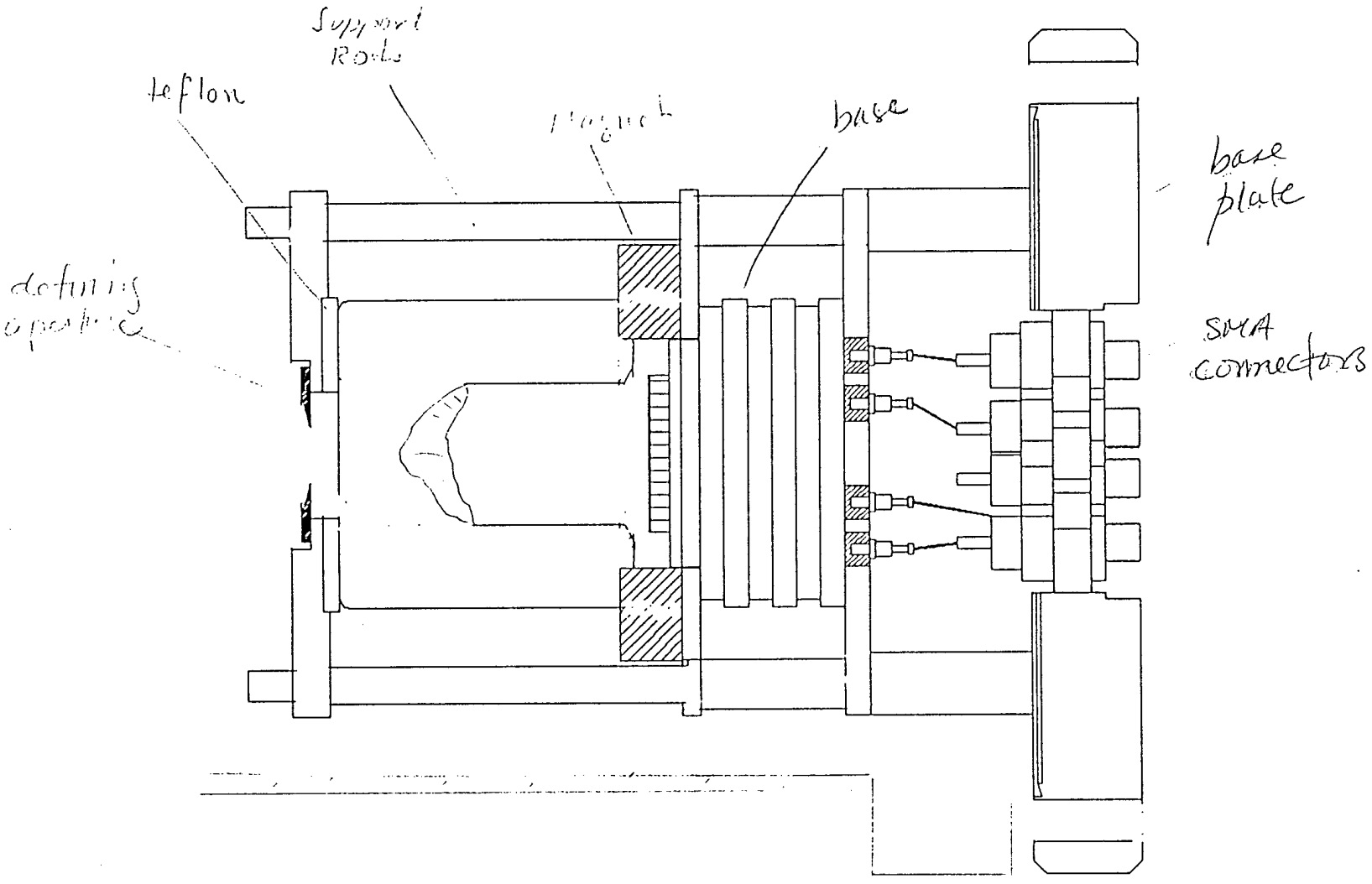
Support Rod
teflon
base
base plate
defining aperture
SMA connectors

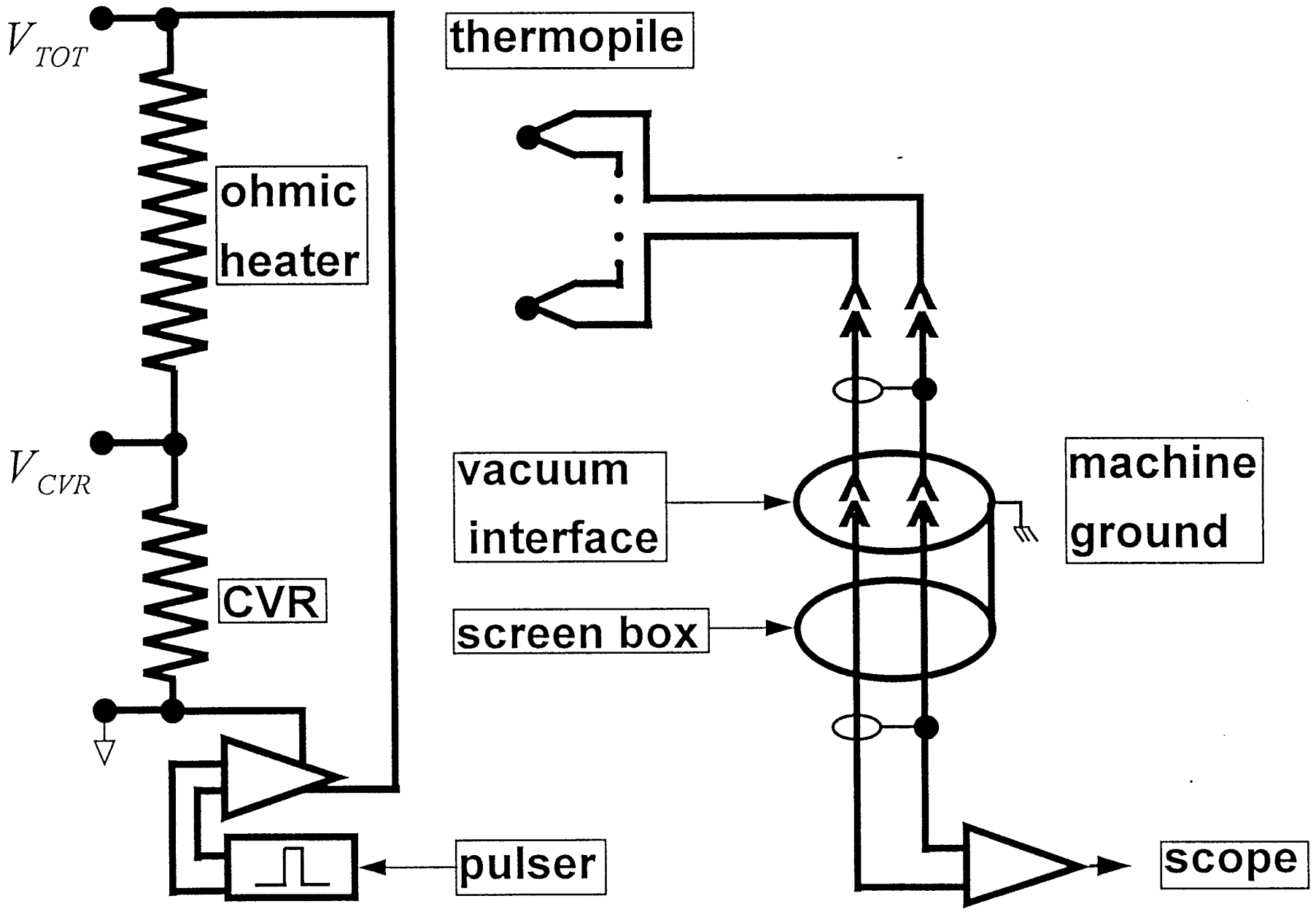
$V_{TOT}$
ohmic heater
$V_{CVR}$
CVR
thermopile
vacuum interface
machine ground
screen box
pulser
scope

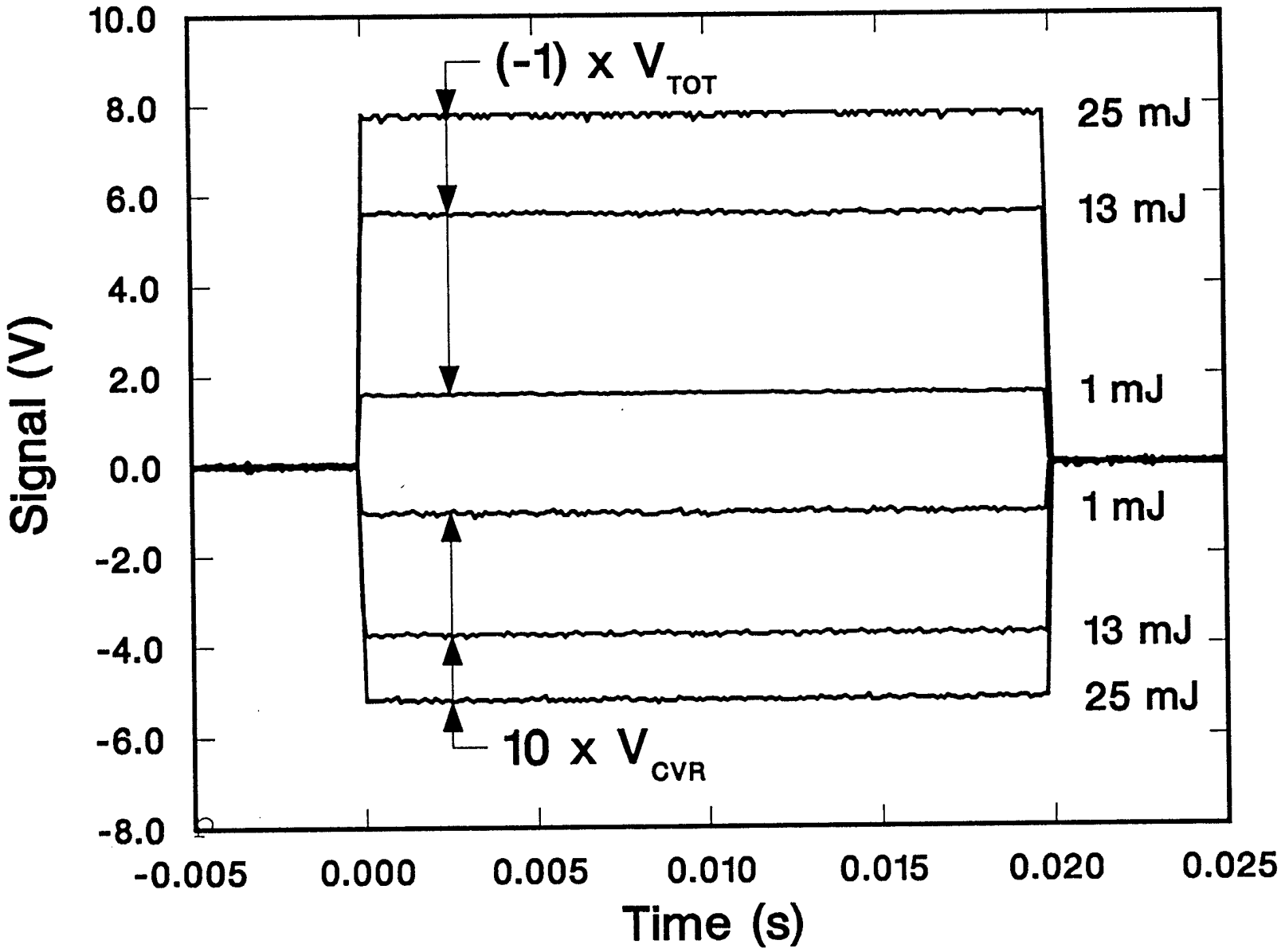
10.0
8.0
6.0
4.0
2.0
0.0
-2.0
-4.0
-6.0
-8.0
Signal (V)
(-1) x V TOT
25 mJ
13 mJ
1 mJ
1 mJ
13 mJ
25 mJ
10 x V CVR
-0.005
0.000
0.005
0.010
0.015
0.020
0.025
Time (s)

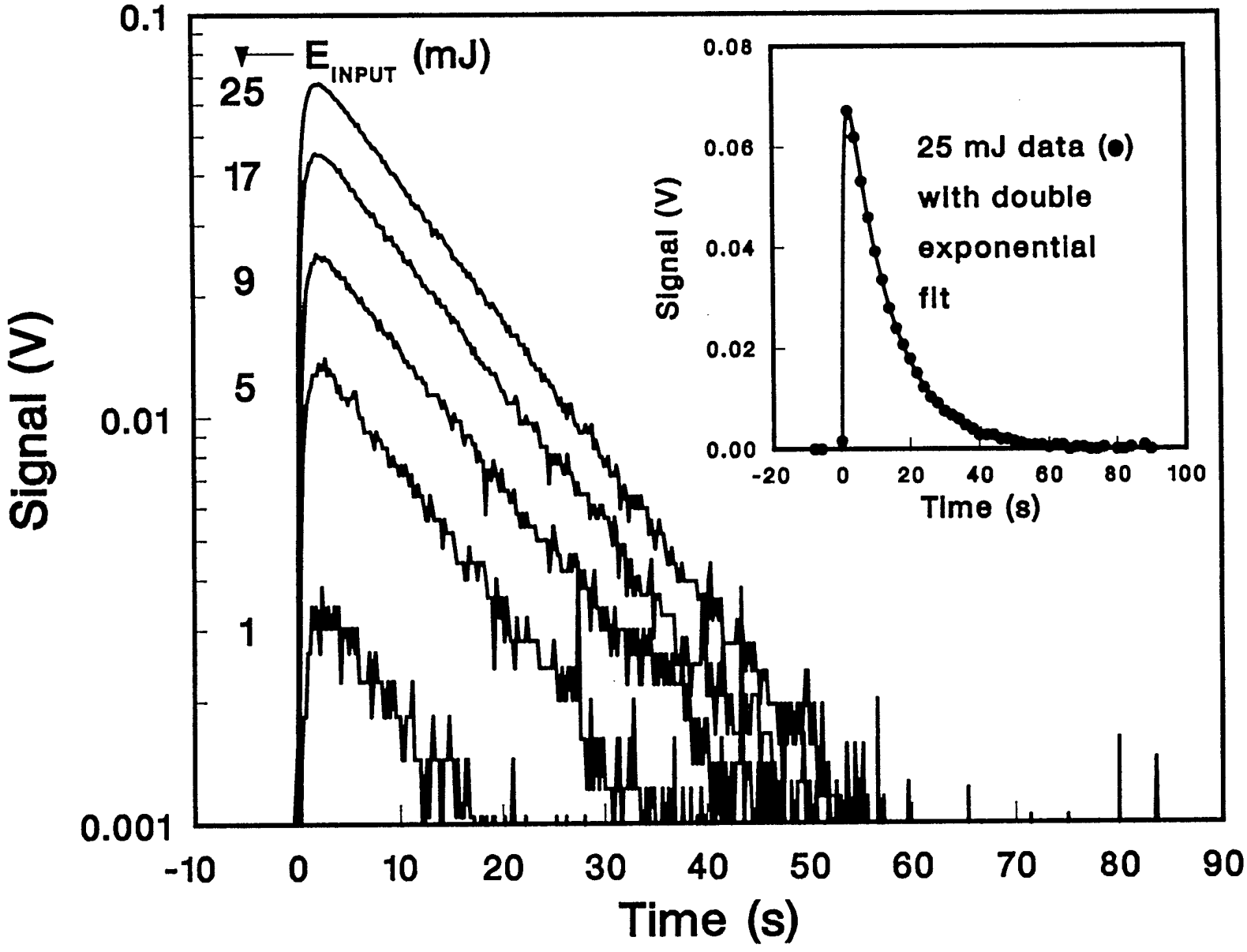
0.1
0.01
0.001
Signal (V)
E INPUT (mJ)
25
17
9
5
1
-10
0
10
20
30
40
50
60
70
80
90
Time (s)
0.08
0.06
0.04
0.02
0.00
Signal (V)
25 mJ data (●)
with double
exponential
fit
-20
0
20
40
60
80
100
Time (s)

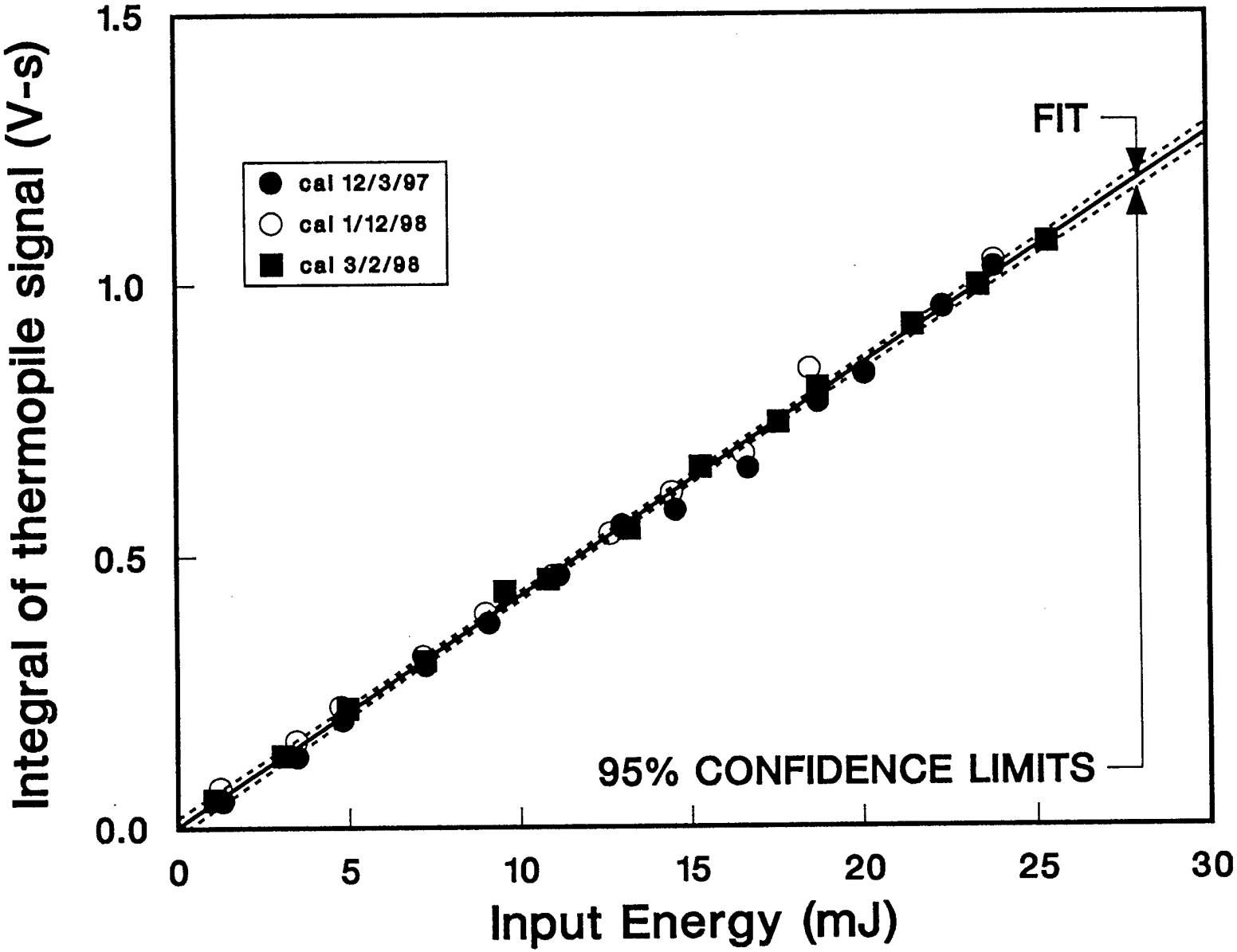
Integral of thermopile signal (V-s)
1.5
1.0
0.5
0.0
0
5
10
15
20
25
30
Input Energy (mJ)
cal 12/3/97
cal 1/12/98
cal 3/2/98
FIT
95% CONFIDENCE LIMITS

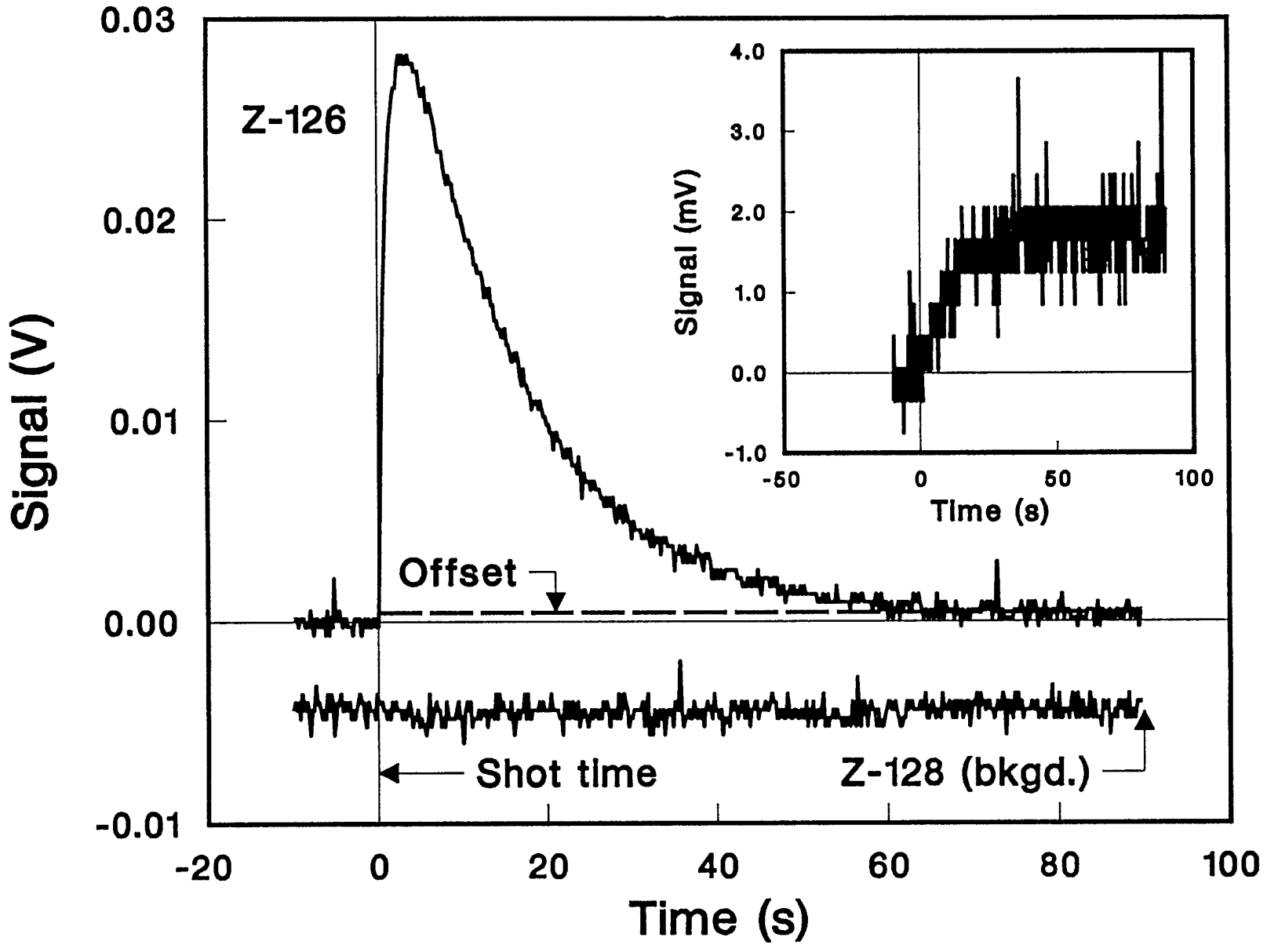
Z-126
Signal (V)
0.03
0.02
0.01
0.00
-0.01
-20
0
20
40
60
80
100
Time (s)
Offset
Shot time
Z-128 (bkgd.)
Signal (mV)
4.0
3.0
2.0
1.0
0.0
-1.0
-50
0
50
100
Time (s)

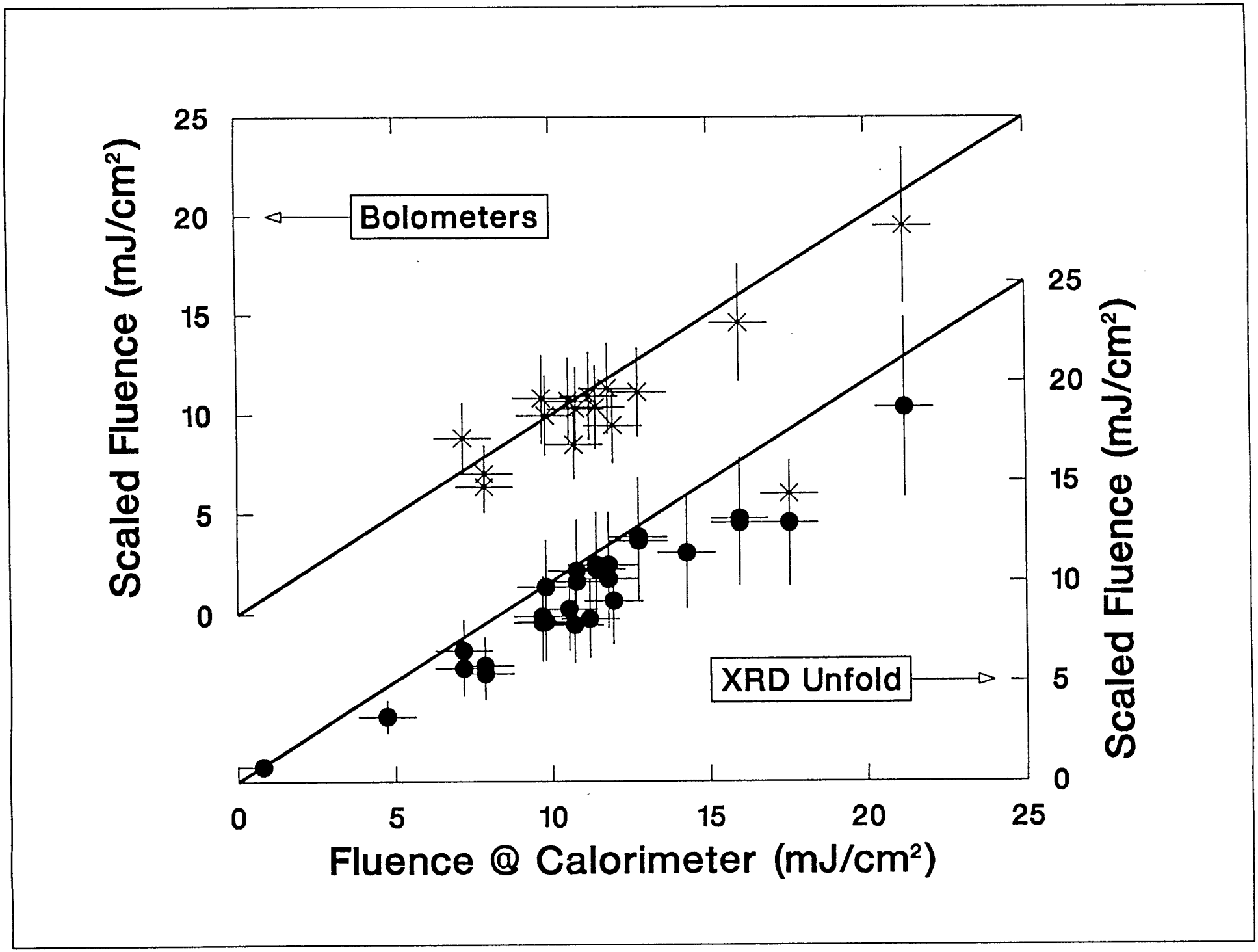
Scaled Fluence (mJ/cm²)
25
20
15
10
5
0
Bolometers
XRD Unfold
25
20
15
10
5
0
Scaled Fluence (mJ/cm²)
0
5
10
15
20
25
Fluence @ Calorimeter (mJ/cm²)

Report Number (14) SAND--98-0555C
CONF-980605--

Publ. Date (11) 199805
Sponsor Code (18) DOE/DP, XF
UC Category (19) UC-700, DOE/ER